Two-photon controlled-phase gates enabled by photonic dimers

Zihao Chen, Yao Zhou, and Jung-Tsung Shen*
Department of Electrical and Systems Engineering, Washington University in St. Louis, St. Louis, Missouri 63130, USA

Pei-Cheng Ku and Duncan Steel
Electrical Engineering and Computer Science Department, University of Michigan, Ann Arbor, Michigan 48109, USA

(Received 19 September 2020; accepted 3 May 2021; published 21 May 2021)

Photons are appealing as flying quantum bits due to their low-noise, long coherence times, light-speed transmission, and ease of manipulation at the single-qubit level using standard optical components such as beam splitters and waveguides. The challenge in optical quantum information processing has been the realization of two-qubit gates for photonic qubits due to the lack of highly efficient optical Kerr nonlinearities at the single-photon level. To date, only probabilistic two-qubit photonic controlled-phase gates based on linear optics and projective measurement using photon detectors have been demonstrated. Here we show that a high-fidelity frequency-encoded deterministic two-photon controlled-phase gate can be achieved by exploiting the strong photon-photon correlation enabled by photonic dimers, and the unique nonreciprocal photonic propagation in chiral quantum nanophotonic systems.

DOI: 10.1103/PhysRevA.103.052610

I. INTRODUCTION

Quantum information science exploits quantum mechanical phenomena such as superposition and entanglement to improve classical communication, information processing, computation, and precision measurement. In quantum information processing, single-qubit operations are not sufficient to unlock all the computational power that is endowed by a collection of qubits. Quantum computation comprised of only single-quantum bit (qubit) operations can be efficiently simulated by a classical architecture. Hence it is necessary and in fact sufficient to add a two-qubit gate such as a controlled-phase (C-phase) gate or its equivalent controlled-NOT (C-NOT) gate to a finite set of single-qubit gates to achieve what no longer can be efficiently simulated on a classical computer. Among all possible physical realizations, optical quantum information science, where photons are used as flying qubits, has attracted significant attentions. Photons are appealing for their low-noise, long coherence times, light-speed transmission, and ease of manipulation at the single-qubit level using standard optical components such as beam splitters and waveguides.

The challenge in optical quantum information processing has been the realization of two-bit photonic gates due to the lack of highly efficient optical Kerr nonlinearities at the single-photon level. To overcome this hurdle, in a breakthrough, Knill, Laflamme, and Milburn (KLM) showed that such an efficient nonlinearity can be achieved using only linear optical elements, auxiliary photons, and projective measurement [1]. Although subsequent developments have reduced the complexity in the measurement-based and teleportation-based KLM protocol such that linear optical quantum computing (LOQC) [2] has become one of the leading candidates for the implementation of large-scale universal quantum computation, the technological requirements such as fast feed-forward and optical quantum memory remain extremely challenging. To date, only probabilistic two-qubit photonic logic gates based on linear optics and projective measurements using photon detectors could be realized. This article proposes a high-fidelity frequency-encoded deterministic two-qubit photonic controlled-phase (controlled-Z) gate. The proposed gate is based on the unique nonlinear phase of two-photon dimers [3–10] and the nonreciprocal photon transport properties in chiral quantum nanophotonic systems [11–13], wherein strong photon-photon correlation and single-photon-level optical nonlinearity can be engineered. We show that in a chiral optical waveguide the formation of the two-photon dimers is efficient and the dimers acquire a nontrivial π phase shift after transmitting through the quantum emitter. We also discuss the experimental configuration for the proposed logic gate.

A deterministic photonic two-qubit gate does not require a substantial resource overhead (e.g., large cluster states or auxiliary single photons) and can have a much higher intrinsic success rate, but the realization necessitates a strong photon-photon correlation and single-photon-level optical nonlinearity. Deterministically, rather than probabilistically, entangling single photons has been recently demonstrated in ultracold atomic systems in the Rydberg blockade regime using electromagnetically induced transparency (EIT) [9,10], wherein the propagation of photon pairs is dominated by a two-photon dimer [3–8]. Other mechanisms to entangle single photons and to generate very large nonlocal nonlinear interactions between pairs of colliding slow-light pulses can be realized in atomic vapors in the regime of electromagnetically induced transparency [14]. Further advances in optical quantum information science can be achieved by producing strong

*jushen@wustl.edu

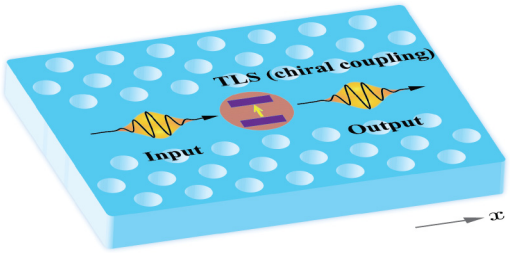

FIG. 1. Schematic diagram of a chiral two-level system (TLS). The chiral photon-quantum dot interaction can be induced via either the Zeeman splitting by a magnetic field [11,13], or by selective placement of the quantum dot at a chiral point in the reciprocal waveguide [12].

photon-photon interactions in solid-state platforms. Semiconductor waveguides offer a tighter photonic confinement such that the interference effect can fundamentally alter the photonic transport [15] and semiconductor platforms can be more easily integrated on a chip to enable a fully scalable quantum architecture.

II. NONTRIVIAL PHOTONIC TRANSMISSION PHASE IN CHIRAL WAVEGUIDES

One of the key enabling features for the proposed controlled-phase gate is the nontrivial phases acquired by incident quantum photonic states transmitting through a chiral two-level system (TLS) (Fig. 1). Chiral photon-quantum emitter interaction can be implemented in reciprocal optical waveguides to realize a chiral quantum nanophotonic system that only permits a unidirectional light propagation [11–13]. The waveguides are single-polarization single-moded (SPSM) waveguide [16] so that there is no mode-conversion and the inter-photon correlations interactions are maximized [17]. For brevity, henceforth the waveguide and the quantum emitter in the chiral configurations will be referred to as the "chiral waveguide" and the "chiral atom," respectively. We note that the fundamental mechanisms of the chiral waveguides are different from those in the photonic topological waveguides with chiral edge channels that provide topological protection against backscattering from disorder [18]. Nonetheless, both the chiral and the photonic topological waveguides support the nontrivial phases for the realization of the phase gate.

Here we describe the emergence of the nontrivial phase for resonant chiral photons (which we shall denote as the $|0\rangle$ qubit). The mechanisms for creating an effective chiral waveguide via the chiral photon-quantum dot couplings are described in Refs. [11–13].

Consider the photon-chiral atom scattering process in a chiral photonic waveguide. The Hamiltonian describing the system is [6,7,19]

$$\begin{aligned} H/\hbar = &\int dx\, c^\dagger(x)(-iv_g\partial_x)c(x) \\ &+ \int dx\, \delta(x)[Vc(x)a_e^\dagger a_g + \text{H.c.}] \\ &+ \omega_g a_g^\dagger a_g + (\omega_e - i\gamma)a_e^\dagger a_e, \end{aligned} \tag{1}$$

where the first term describes the waveguided photons propagating with a group velocity v_g. $c^\dagger(x)$ $[c(x)]$ is the creation (annihilation) operator for the unidirectional (right-moving in this case) photon at position x. The next term describes the absorption of a photon and the excitation of the chiral atom from the ground state to the excited state with a coupling strength V. $a_{g,e}^\dagger$ $(a_{g,e})$ is the creation (annihilation) operator of the corresponding atomic ground and excited state, respectively. The H.c. term refers to the hermitian conjugate and describes the time-reversed relaxation process with an emitted photon. The last two terms describe the energy of the atomic states. $\Omega = \omega_e - \omega_g$ is the transition frequency of the atom and γ is the dissipation of the excited state [19–21]. The decay rate of the excited states into the waveguided mode is $\Gamma = V^2/v_g$ and the spontaneous emission lifetime of the atom is $\tau_0 = 1/\Gamma$.

A photonic input state is "mapped" by the chiral atom into an output state. The transmission amplitude of the photonic input through the chiral atom depends on the nature of the photonic state. In particular, for a multiphoton input, the correlated transport due to the photon-chiral atom interactions can induce a non-trivial nonlinear phase shift in the transmission amplitude. In the following, we start by discussing the transmission phases of various monochromatic photonic inputs, followed by a detailed discussion of the realistic cases when the inputs are wave packets with a finite bandwidth.

A. Monochromatic inputs

Single-photon input. The transmission amplitude for a single-photon input of frequency ω is [6,7]

$$t_\omega = \frac{\omega - (\Omega - i\gamma) - i\Gamma/2}{\omega - (\Omega - i\gamma) + i\Gamma/2}. \tag{2}$$

For a far-detuned photon ($|\omega - \Omega| \gg \gamma, \Gamma$), the transmission phase is trivially 0 ($t_\omega \approx +1 = e^{i0}$). For a resonant photon ($\omega \approx \Omega$), however, $t_\omega \approx -1 = e^{i\pi}$ when $\gamma \ll \Gamma$ and consequently the transmitted photon acquires a π phase shift.

Two-photon input. In a chiral waveguide, there are two 2-photon eigenstates of the scattering matrix $\mathbb{S}$ [6,7]: (i) a two-photon plane-wave state $|W_{\omega_1,\omega_2}\rangle$ which describes independent (uncorrelated) photon transport and has a transmission amplitude that is a product of the two single-photon transmission amplitudes: $t_W = t_{\omega_1} \times t_{\omega_2}$; and (ii) a two-photon dimer state $|B_{2\omega}\rangle$ which describes correlated photon transport and has a transmission amplitude

$$t_B = \frac{2\omega - 2(\Omega - i\gamma) - i2\Gamma}{2\omega - 2(\Omega - i\gamma) + i2\Gamma}. \tag{3}$$

The formation of a photonic dimer via a Fock state containing two independent photons manifests the most fundamental quantum nonlinear optical $\chi^{(3)}$ process. The existence of the photonic dimers have been experimentally confirmed [9,10]. For an input of resonant two-photon plane-wave state $|W_{\omega_1,\omega_2}\rangle$ $(\omega_1 \approx \omega_2 \approx \Omega)$, the transmission amplitude $t_W \approx (-1)^2 = 1$ (trivial two-photon phase 0), while an input of resonant two-photon dimer $|B_{2\omega}\rangle$ $(\omega \approx \Omega)$ has a transmission amplitude ≈ -1 (nonlinear two-photon phase π) when $\gamma \ll \Gamma$. The two-photon dimer $|B_{2\omega}\rangle$ furnishes the set of quantum states with the desired transformation property for the controlled-phase gate. We note that the mechanism in Ref. [14] can also yield a

homogeneous conditional phase shift of π for weakly focused single-photon pulses.

Nonresonant photons. For non-resonant photons, due either to frequency detuning, or to mismatch of polarization or other characteristics, each transmitted photon has a transmission amplitude 1 and thus acquires a trivial phase 0.

B. Wave-packet inputs with a finite bandwidth

In practice, the photonic inputs are always in wave-packet forms and, more importantly, the performance of the quantum photonic devices in general attains the maximum when the properties of the wave packets (e.g., the center frequency and the bandwidth) meet certain working conditions, especially when dissipations are present. Recent experimental advances in single-photon pulse shaping has made it possible to control and generate single-photon wave packets from a timescle of 0.1–1 μs [22,23] to ∼80 ps [24] (i.e., controllable bandwidth up to ∼10 GHz). For this purpose, in addition to the heuristic analysis for the monochromatic inputs that motivated the design of the controlled-phase logic gate, we also undertake a computational approach to research the controlled-phase gate when the inputs are wave packets with a finite bandwidth. In the computational approach, the equations of motion, governed by the Hamiltonian in Eq. (1), are evolved numerically in time to trace out the full spatiotemporal dynamics of the scattering process. The numerical approach employs standard numerical discretization and is independent of any ansatz adopted in the analytical approach; thus the numerical results provide an independent check of the analytical predictions. We first consider the case when a single resonant photon is injected from the left in the chiral waveguide in Fig. 1. The incident photon is described by a finite-bandwidth Gaussian pulse $\phi_{\rm in}(x) = \frac{1}{(2\pi\sigma)^{1/4}} e^{-\frac{(x-x_o)^2}{4\sigma^2} + ik_o x}$, where σ is the spatial width, x_o is the initial position, and $k_o v_g (= \Omega)$ is the center frequency of the Gaussian pulse. Here the pulse propagates in the chiral waveguide with an effective index n_{eff} which can be controlled by the slow-light waveguide structures [25–27], providing further pulse-shaping capability for manipulating the pulse temporal and spatial widths. After scattering, the phase shift $\theta(x)$ acquired by the transmitted photon $\phi_{\rm out}(x)$ is obtained by $\theta(x) = \arg[\phi_{\rm out}(x)/\phi_{\rm ref}(x)]$, where $\phi_{\rm ref}(x)$ is a reference wave function describing a resonant photon undergoing free propagation ($\Gamma = 0$).

Figure 2(a) plots the probability density (amplitude square) of the incoming and outgoing photons, respectively, when the size of the input photon wave packet satisfies $\sigma = 1.5 v_g/\Gamma$ (for instance, if the quantum emitter's spontaneous emission time is $1/\Gamma \approx 0.1$ ns, the pulse duration is $\sim 6\sigma/v_g \approx 0.9$ ns). The single-photon phase shift (green curve) is numerically found to be π, as predicted by Eq. (2). Next, consider a resonant two-photon Gaussian Fock state input: $\phi_{\rm in}(x_1, x_2) = \frac{1}{(2\pi\sigma)^{1/2}} e^{-\frac{(x_1-x_o)^2}{4\sigma^2} - \frac{(x_2-x_o)^2}{4\sigma^2} + ik_o(x_1+x_2)}$. Each photon wave packet satisfies $\sigma = 1.5 v_g/\Gamma$. Figure 2(b) plots the two-photon probability density of the scattering process (please see Ref. [28] for details of the graphic representation): the probability density of the two-photon Gaussian input is a disk in the third quadrant ($x_1, x_2 < 0$), while the density of the outgoing two-photon state in the first quadrant is concentrated along the diagonal, indicating a bunching behavior and the formation of photonic dimer. The output state is a linear superposition of both $|W_{\omega_1,\omega_2}\rangle_{\omega_1 \approx \omega_2}$ and $|B_{2\omega}\rangle$. Figure 2(c) plots the two-photon phase shift of the outgoing two-photon state by $\theta(x_1, x_2) = \arg[\phi_{\rm out}(x_1, x_2)/\phi_{\rm ref}(x_1, x_2)]$. Numerically, it is found that the two-photon phase shift takes only discrete values and is either π (green region) or 0 (blue regions), for all x_1 and x_2. The π phase shift is contaminated by the 0 phase shift due to the emergence of the two-photon plane-wave states. The average phase shift is obtained by averaging over the first quadrant. For example, for the two-photon nonlinear phase, $\theta_2 \equiv \frac{\iint dx_1 dx_2 \theta(x_1,x_2)|\phi_{\rm out}(x_1,x_2)|^2}{\iint dx_1 dx_2 |\phi_{\rm out}(x_1,x_2)|^2}$. The optimal wave-packet characteristics, $\sigma = 1.5 v_g/\Gamma$, is determined computationally so that the fidelity is maximized and the errors of the nonlinear phases relative to π are minimized, as shown in Sec. IV.

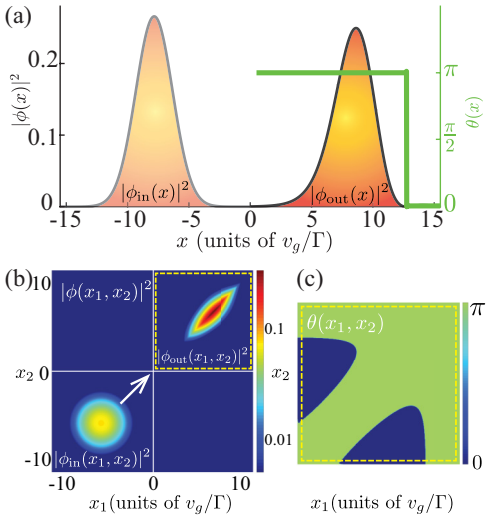

FIG. 2. Probability density plot and phase shift for resonant photons. (a) Single-photon case. Green curve indicates the numerical π phase shift. (b) Density plot for the two-photon case. (c) Phase shift of the outgoing two-photon state. Parameters for the scattering processes: $\sigma = 1.5 v_g/\Gamma$ (for instance, if the atomic spontaneous emission time is $1/\Gamma \approx 0.1$ ns, the pulse duration is $6\sigma/v_g \approx 0.9$ ns), and $\gamma = 0$.

III. TWO-PHOTON CONTROLLED-PHASE GATE ARCHITECTURE

The controlled-phase gate performs a conditional phase shift on the input states so that $|x\rangle|y\rangle \to e^{i\theta_{xy}}|x\rangle|y\rangle$ ($x, y = 0, 1$), where $\theta_{00} + \theta_{11} \neq \theta_{10} + \theta_{01}$. [29]. The unitary transformations of the photonic states in a chiral waveguide provides a mechanism for realizing a controlled-π-phase (control-Z) gate so that $\theta_{11} = 0$, and $\theta_{00} = \theta_{10} = \theta_{01} = \pi$. Figure 3 shows schematically the proposed controlled-phase gate. The architecture of the four-port gate is a Mach-Zender interferometer (MZI), similar to that proposed by Söllner *et al* in Ref. [11] but here with a segment of chiral waveguide (Fig. 1) embedded in the central region of each path. The input qubits are frequency encoded: $|0\rangle$ represents a resonant photon with a frequency $\omega_0 \approx \Omega$, the transition frequency of the chiral atom, while $|1\rangle$ represents an off-resonant photon with a frequency

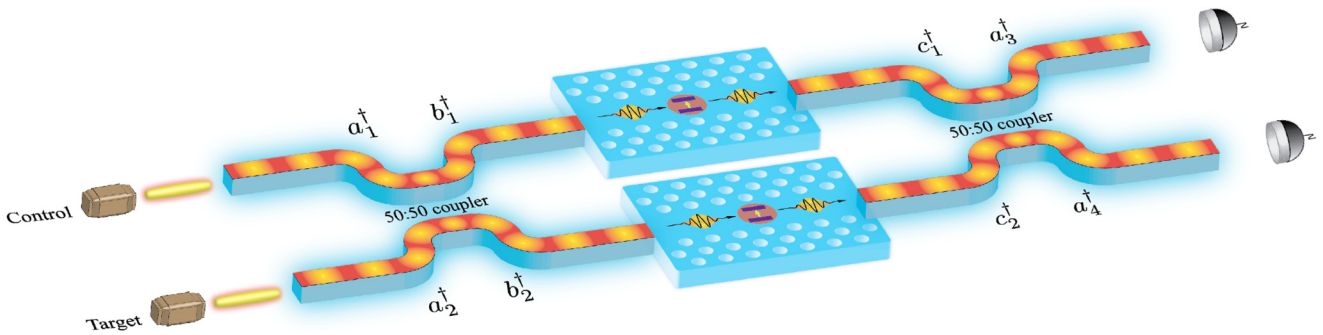

FIG. 3. Schematic diagram of the two-photon controlled-phase gate.

ω_1 such that $|\omega_1 - \Omega| \gg \Gamma, \gamma$. The input ports are coupled by a 50:50 couplers, as are the output ports. The couplers transform the the optical fields linearly as follows $a_1^\dagger = (b_2^\dagger - b_1^\dagger)/\sqrt{2}$, $a_2^\dagger = (b_2^\dagger + b_1^\dagger)/\sqrt{2}$, $c_1^\dagger = (a_4^\dagger - a_3^\dagger)/\sqrt{2}$, $c_2^\dagger = (a_4^\dagger + a_3^\dagger)/\sqrt{2}$. We note that a typical commercially available coupler has a wide working bandwidth of ≈100 nm at telecommunication bands so that the couplers are able to function for both qubits. Two independent photonic qubits are fed into the input ports. We now describe the gate operation by explicitly enumerating the mapping of the four input states.

(1) $|1\rangle_{a_1}|1\rangle_{a_2} \to |1\rangle_{a_3}|1\rangle_{a_4}$. The input state consists of one off-resonant photon $|1\rangle$ in each input port: $|\text{in}\rangle = |1\rangle_{a_1}|1\rangle_{a_2} = a^\dagger_{1,\omega_1}a^\dagger_{2,\omega_1}|\varnothing\rangle$, where $|\varnothing\rangle$ is photonic vacuum state. After the coupler, the state transforms into $\frac{1}{2}(b^{\dagger 2}_{2,\omega_1} - b^{\dagger 2}_{1,\omega_1})|0\rangle$. The off-resonant photons transmit through the chiral atoms freely so that $b^\dagger_{1,\omega_1} \to c^\dagger_{1,\omega_1}$, $b^\dagger_{2,\omega_1} \to c^\dagger_{2,\omega_1}$ and the output state is $|\text{out}\rangle = \frac{1}{2}(c^{\dagger 2}_{2,\omega_2} - c^{\dagger 2}_{1,\omega_1})|\varnothing\rangle = a^\dagger_{3,\omega_1}a^\dagger_{4,\omega_1}|\varnothing\rangle = |1\rangle_{a_3}|1\rangle_{a_4}$.

(2) $|0\rangle_{a_1}|1\rangle_{a_2} \to -|0\rangle_{a_3}|1\rangle_{a_4}$. The input state consists of one resonant photon $|0\rangle$ in the control port and one off-resonant photon $|1\rangle$ in the target port: $|\text{in}\rangle = |0\rangle_{a_1}|1\rangle_{a_2} = a^\dagger_{1,\omega_0}a^\dagger_{2,\omega_1}|\varnothing\rangle$. After the coupler, the state transforms into $\frac{1}{2}(b^\dagger_{2,\omega_0} - b^\dagger_{1,\omega_0})(b^\dagger_{2,\omega_1} + b^\dagger_{1,\omega_1})|\varnothing\rangle$. The $|1\rangle$ qubit again transforms trivially; in contrast, for the $|0\rangle$ bit, due to the π phase shift through the chiral atom, the photonic field transforms as $b^\dagger_{1,\omega_0} \to -c^\dagger_{1,\omega_0}$, $b^\dagger_{2,\omega_0} \to -c^\dagger_{2,\omega_0}$, and the output is $|\text{out}\rangle = -\frac{1}{2}(c^\dagger_{2,\omega_0} - c^\dagger_{1,\omega_0})(c^\dagger_{2,\omega_1} + c^\dagger_{1,\omega_1})|\varnothing\rangle = -a^\dagger_{3,\omega_0}a^\dagger_{4,\omega_1}|\varnothing\rangle = -|0\rangle_{a_3}|1\rangle_{a_4}$.

(3) Similarly $|1\rangle_{a_1}|0\rangle_{a_2} \to -|1\rangle_{a_3}|0\rangle_{a_4}$.

(4) $|0\rangle_{a_1}|0\rangle_{a_2} \to -|0\rangle_{a_3}|0\rangle_{a_4}$. The input has one resonant photon in each port: $|\text{in}\rangle = |0\rangle_{a_1}|0\rangle_{a_2} = a^\dagger_{1,\omega_0}a^\dagger_{2,\omega_0}|\varnothing\rangle$. After the coupler, the state turns into $\frac{1}{2}(b^{\dagger 2}_{2,\omega_0} - b^{\dagger 2}_{1,\omega_0})|\varnothing\rangle$, which is a linear superposition of Fock states in the arms, each containing two resonant photons. The uncorrelated two-photon Fock states can be decomposed by the complete set of bases $|B_{2\omega}\rangle$ and $|W_{\omega_1,\omega_2}\rangle_{\omega_1\approx\omega_2}$. The two photons in the $|B_{2\omega}\rangle$ state acquire a π phase shift collectively, thus $b^{\dagger 2}_{1,\omega_0} \to -c^{\dagger 2}_{1,\omega_0}$, $b^{\dagger 2}_{2,\omega_0} \to -c^{\dagger 2}_{2,\omega_0}$, giving to the output state a contribution $-\frac{1}{2}(c^{\dagger 2}_{2,\omega_0} - c^{\dagger 2}_{1,\omega_0})|\varnothing\rangle = -a^\dagger_{3,\omega_0}a^\dagger_{4,\omega_0}|\varnothing\rangle = -|0\rangle_{a_3}|0\rangle_{a_4}$, with a desired π phase shift. In contrast, the two photons in the $|W_{\omega_1,\omega_2}\rangle_{\omega_1\approx\omega_2}$ acquire an unwanted 0 phase shift collectively $(\pi + \pi \bmod 2\pi)$.

Using four orthogonal bases $|00\rangle$, $|01\rangle$, $|10\rangle$, and $|11\rangle$, the gate operation can be summarized by

$$U = \begin{bmatrix} -1 & & & \\ & -1 & & \\ & & -1 & \\ & & & 1 \end{bmatrix} = (-1) \times \begin{bmatrix} 1 & & & \\ & 1 & & \\ & & 1 & \\ & & & -1 \end{bmatrix}, \tag{4}$$

Thus, the transformation of the four orthogonal bases $|00\rangle$, $|01\rangle$, $|10\rangle$, and $|11\rangle$ constitutes the two-photon controlled-phase gate operation subject to a trivial global phase π. Such a global phase can be readily rectified by adding one wide-bandwidth $\pi/2$ phase shifter on each arm.

IV. FIDELITY ANALYSIS

A. Average gate fidelity

To characterize the similarity between the experimentally implemented quantum logic gate in a particular model and the ideal gate, we numerically compute the average gate fidelity

$$\bar{F} = \overline{\langle\chi_{\text{in}}|\hat{U}^\dagger_{\text{ideal}}\rho_{\text{out}}\hat{U}_{\text{ideal}}|\chi_{\text{in}}\rangle}, \tag{5}$$

where the overline denotes the average over all possible input states $|\chi_{\text{in}}\rangle$, and $\hat{U}_{\text{ideal}}$ is the unitary operator corresponding to the ideal gate [30,31]. $\bar{F}$ can be calculated directly via quantum process tomography. For the two-photon controlled-phase gate, for an input state $|\chi_{\text{in}}\rangle = u_{00}|00\rangle + u_{01}|01\rangle + u_{10}|10\rangle + u_{11}|11\rangle$ (subject to the normalization condition $|u_{00}|^2 + |u_{01}|^2 + |u_{10}|^2 + |u_{11}|^2 = 1$), the two-photon wave function at each stage when propagating in the logic gate is given by

$$\begin{aligned}
|\chi_{\text{in}}\rangle &= u_{00}|00\rangle + u_{01}|01\rangle + u_{10}|10\rangle + u_{11}|11\rangle \\
&= u_{00}a^\dagger_{1,\omega_0}a^\dagger_{2,\omega_0}|\varnothing\rangle + u_{01}a^\dagger_{1,\omega_0}a^\dagger_{2,\omega_1}|\varnothing\rangle + u_{10}a^\dagger_{1,\omega_1}a^\dagger_{2,\omega_0}|\varnothing\rangle + u_{11}a^\dagger_{1,\omega_1}a^\dagger_{2,\omega_1}|\varnothing\rangle \\
&\xrightarrow{\text{firstcoupler}} \frac{u_{00}}{2}\left(b^\dagger_{2,\omega_0} - b^\dagger_{1,\omega_0}\right)\left(b^\dagger_{2,\omega_0} + b^\dagger_{1,\omega_0}\right)|\varnothing\rangle + \frac{u_{01}}{2}\left(b^\dagger_{2,\omega_0} - b^\dagger_{1,\omega_0}\right)\left(b^\dagger_{2,\omega_1} + b^\dagger_{1,\omega_1}\right)|\varnothing\rangle \\
&\quad + \frac{u_{10}}{2}\left(b^\dagger_{2,\omega_1} - b^\dagger_{1,\omega_1}\right)\left(b^\dagger_{2,\omega_0} + b^\dagger_{1,\omega_0}\right)|\varnothing\rangle + \frac{u_{11}}{2}\left(b^\dagger_{2,\omega_1} - b^\dagger_{1,\omega_1}\right)\left(b^\dagger_{2,\omega_1} + b^\dagger_{1,\omega_1}\right)|\varnothing\rangle
\end{aligned}$$

$$\begin{aligned}
&\xrightarrow{\text{atom}} \frac{u_{00}}{2}t_2e^{i\theta_2}\left(c^\dagger_{2,\omega_0}-c^\dagger_{1,\omega_0}\right)\left(c^\dagger_{2,\omega_0}+c^\dagger_{1,\omega_0}\right)|\varnothing\rangle+\frac{u_{01}}{2}t_1e^{i\theta_1}\left(c^\dagger_{2,\omega_0}-c^\dagger_{1,\omega_0}\right)\left(c^\dagger_{2,\omega_1}+c^\dagger_{1,\omega_1}\right)|\varnothing\rangle\\
&+\frac{u_{10}}{2}t_1e^{i\theta_1}\left(c^\dagger_{2,\omega_1}-c^\dagger_{1,\omega_1}\right)\left(c^\dagger_{2,\omega_0}+c^\dagger_{1,\omega_0}\right)|\varnothing\rangle+\frac{u_{11}}{2}\left(c^\dagger_{2,\omega_1}-c^\dagger_{1,\omega_1}\right)\left(c^\dagger_{2,\omega_1}+c^\dagger_{1,\omega_1}\right)|\varnothing\rangle\\
&\xrightarrow{\text{secondcoupler}} u_{00}t_2e^{i\theta_2}a^\dagger_{3,\omega_0}a^\dagger_{4,\omega_0}|\varnothing\rangle+u_{01}t_1e^{i\theta_1}a^\dagger_{3,\omega_0}a^\dagger_{4,\omega_1}|\varnothing\rangle+u_{10}t_1e^{i\theta_1}a^\dagger_{3,\omega_1}a^\dagger_{4,\omega_0}|\varnothing\rangle+u_{11}a^\dagger_{3,\omega_1}a^\dagger_{4,\omega_1}|\varnothing\rangle\\
&=u_{00}t_2e^{i\theta_2}|00\rangle+u_{01}t_1e^{i\theta_1}|01\rangle+u_{10}t_1e^{i\theta_1}|10\rangle+u_{11}|11\rangle=|\chi_{\text{out}}\rangle, \qquad (6)
\end{aligned}$$

where single- and two-photon quantum processes are denoted by $b^\dagger_{i,\omega_0}\to t_1e^{i\theta_1}c^\dagger_{i,\omega_0}$ and $b^\dagger_{i,\omega_0}b^\dagger_{i,\omega_0}\to t_2e^{i\theta_2}c^\dagger_{i,\omega_0}c^\dagger_{i,\omega_0}$, respectively. The transmission amplitudes t_i and the phase shift θ_i are averaged over the positive x axis (for $i=1$) or the first quadrant (for $i=2$). For example, $t_2=\sqrt{\iint|\phi_{\text{out}}(x_1,x_2)|^2dx_1dx_2}$ and $\theta_2=\frac{\iint dx_1dx_2\theta(x_1,x_2)|\phi_{\text{out}}(x_1,x_2)|^2}{\iint dx_1dx_2|\phi_{\text{out}}(x_1,x_2)|^2}$.

Thus, from

$$\begin{aligned}
|\chi_{\text{out}}\rangle&=u_{00}t_2e^{i\theta_2}|00\rangle+u_{01}t_1e^{i\theta_1}|01\rangle\\
&\quad+u_{10}t_1e^{i\theta_1}|10\rangle+u_{11}|11\rangle\\
\hat{U}_{\text{ideal}}|\chi_{\text{in}}\rangle&=u_{00}|00\rangle+u_{01}|01\rangle+u_{10}|10\rangle-u_{11}|11\rangle,
\end{aligned}$$

it can be shown straightforwardly that the average gate fidelity is reduced to

$$\bar{F}=\overline{||u_{00}|^2t_2e^{i\theta_2}+(|u_{01}|^2+|u_{10}|^2)t_1e^{i\theta_1}-|u_{11}|^2|^2}. \qquad (7)$$

For an ideal logic gate, $t_1=t_2=1,\theta_1=\theta_2=\pi$, it is easily seen that $\bar{F}=1$, as expected.

B. Quantum state tomography of frequency-encoded qubits

The quantum state tomography is powerful methods for probing a quantum state. As laid out in Ref. [32], the measurement relies on performing single-qubit operations in the respective qubit ports. By performing σ_x operations in frequency space and performing a coincidence measurement, the signal intensity is proportional to the projection of density matrix ρ_{out} onto a combined measurement basis $\sigma_x\otimes\sigma_x$ [32]: coincidence signal $\propto\frac{1}{4}\text{Tr}[\rho_{\text{out}}\sigma_x\otimes\sigma_x]=\frac{1}{4}[u_{00}u^*_{11}t_2e^{i\theta_2}+u_{01}u^*_{10}t_1^2+u^*_{01}u_{10}t_1^2+u_{11}u^*_{10}t_1e^{-i\theta_1}]$

In-state average. Following the standard approach [33,34], the input-state average is performed through a random sampling approach on the two-qubit hyper-Bloch sphere, by parametrization of the two-photon input-state on a six-dimensional manifold as

$$u_{00}=\cos\alpha_1, \qquad (8)$$

$$u_{01}=\sin\alpha_1\cos\alpha_2e^{i\phi_1}, \qquad (9)$$

$$u_{10}=\sin\alpha_1\sin\alpha_2\cos\alpha_3e^{i\phi_2}, \qquad (10)$$

$$u_{11}=\sin\alpha_1\sin\alpha_2\sin\alpha_3e^{i\phi_3}, \qquad (11)$$

where $\alpha_{1,2,3}\in[0,\pi/2]$ and $\phi_{1,2,3}\in[0,2\pi]$. Four complex coefficients u_{00}, u_{01}, u_{10}, and u_{11} subject to the normalization condition and the trivial global phase leaves six degrees of freedom. We uniformly sample N points on the six-dimensional numerical mesh $\{\alpha_i,\phi_j\}$, and calculate the average fidelity using all possible N^6 combinations. Numerically, it is found that the relative error of $\bar{F}$ for $N=15$ ($N^6\sim10^7$) and for $N=25$ ($N^6\sim2\times10^8$) is smaller than $<0.5\%$ for typical values of $\sigma\Gamma/v_g$, indicating that the numerical convergence of the values of the fidelity; hereafter we will take $N=15$ for further numerical investigations.

C. Effects of pulse bandwidth and dissipations

Using the average gate fidelity expression [Eq. (7)] and the random sampling approach on the two-qubit hyper Bloch sphere [Eq. (8)], the average gate fidelity $\bar{F}$ can be computationally evaluated as a function of the input wave-packet bandwidth and the gate characteristics.

Effects of pulse bandwidth. Figure 4(a) plots the fidelity $\bar{F}$ as a function of the pulse width σ. For small values of σ, the frequency bandwidth is large so that the off-resonant frequency components degrade the fidelity, even though the center frequency k_0v_g is on resonance. For large values of σ, we found numerically that the weight of the two-photon plane waves in the output state also increases, which also degrades the fidelity. High fidelity $\bar{F}>0.99$ can be achieved when $\sigma\Gamma/v_g$ (the extension of the pulse expressed in the units of spontaneous emission length scale) is in the intermediate range between 0.6 to 2.5. Figure 4(b) plots the phase shift for varying pulse width σ. For large σ (thus narrow frequency band), the single-photon phase shift (blue curve) is π, as

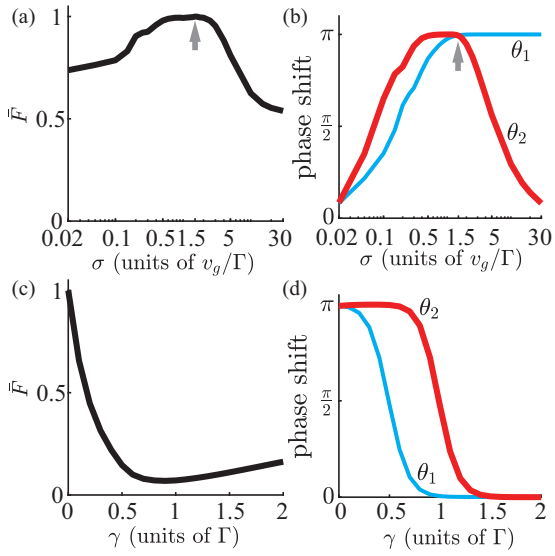

FIG. 4. Numerical results of average gate fidelity $\bar{F}$ and phase shift θ_1, θ_2. (a) $\bar{F}$ and (b) θ_1, θ_2 as a function of photon pulse width σ in the absence of atomic dissipation $\gamma=0$. (c) $\bar{F}$ and (d) θ_1, θ_2 as a function of atomic dissipation γ at $\sigma\Gamma/v_g=1.5$.

expected. The qualitative behavior of the two-photon phase shift θ_2 follows that of the fidelity for the same physical reasons and θ_2 approaches π for the same range of σ. At the optimal pulse duration $\sigma\Gamma/v_g \approx 1.5$, $\theta_1 = 1.00\pi$, $\theta_2 = 0.99\pi$, and $\bar{F} = 99.95\%$.

Effects of dissipation. Here we study the effects of atomic dissipation γ at the optimal pulse duration $\sigma\Gamma/v_g = 1.5$. As plotted in Fig. 4(c), as γ increases, $\bar{F}$ drops gradually and reaches the minimum at around $\gamma = 0.5\Gamma$, at which the phase shift θ_1 for an on-resonant photon has a jump from π to 0 [see Eq. (2)], as shown in Fig. 4(d). The drop is not abrupt as the photons are not monochromatic but have a finite bandwidth. $\bar{F}$ remains low when $\gamma > \Gamma$ as the two-photon phase shift θ_2 has a jump at $\gamma = \Gamma$ [see Eq. (3)], as shown in Fig. 4(d) (red curve). Finally, when $\gamma \gg \Gamma$, $\bar{F} \to 1/4$ because, at large dissipation limit, only the trivial mapping $|11\rangle \to |11\rangle$ that involves off-resonant photons survives.

Estimates of the average gate fidelity. The proposed two-photon controlled-phase gate has yet to be implemented. Nonetheless, here we provide a figure of merit estimate to characterize the performance of the device, using the experimental numbers extracted from relevant experiments. Recently, it is shown that a quantum emitter (InAs/GaAs quantum dot) can be efficiently coupled to a photonic crystal waveguide as the waveguided mode at the band edge is close to a cavity mode to effectively introduce the Purcell effect [35]. The atomic spontaneous decay rate into the waveguided and nonwaveguided modes are given by $\Gamma \approx 6.28\,\text{GHz}$ and $\gamma \approx 0.098\,\text{GHz}$, respectively. Thus one has that $\gamma/\Gamma \approx 0.02$. Consider an optical pulse of temporal duration $6\sigma/v_g \approx 1.43\,\text{ns}$ (where $>99\%$ energy is confined), $\sigma\Gamma/v_g \approx 1.5$. Through the computational tool, one obtains that $t_1 = 93.97\%$, $\theta_1 = 0.99\pi$, $t_2 = 95.80\%$, $\theta_2 = 0.99\pi$, and $\bar{F} = 91.48\%$.

V. EXPERIMENTAL IMPLEMENTATION OF THE CONTROLLED-PHASE GATE

One possible implementation of the controlled phase gate will be based on a photonic crystal (PhC) waveguide featuring a glide plane structure incorporating a dipole emitter such as an InGaAs quantum dot or a defect state in single-walled carbon nanotubes [6,7,11,12,36]. The latter has recently been shown to be a promising quantum emitter at telecom wavelengths and for work near room temperature, while the former is technologically mature due to its good coherence and large oscillator strengths. Polarization or wavelength selectivity can be arranged using either a negatively charged dot as demonstrated in Ref. [12] or a positively charged dot as used by Ref. [11] with an applied magnetic field. A variety of other nanophotonic waveguide structures such as suspended nanowire waveguides [12] can also be used to facilitate the chiral photon-emitter interaction. The dipole emitter is placed at a chiral point where the forward-propagating mode matches with the emission polarization of the dipole emitter. For example, we can drive the dipole emitter in the Faraday configuration and make the $|0\rangle$ photon in resonance with the σ^+ transition. In the implementation of the controlled phase gate, the $|1\rangle$ photon will be detuned from and therefore does not interact with the dipole emitter. In addition, the efficient coupling between the chiral PhC waveguide and the dipole emitter maximizes the gate fidelity [12,35]. In this scheme, the glide plane PhC waveguide section will be adiabatically coupled to a regular PhC waveguide which will then be coupled to a ridge waveguide as part of the MZI. The advantage of choosing a PhC waveguide structure is clear here that the adiabatic transition can allow us to minimize the mode-mismatching losses between different sections, and the glide plane PhC section shifts the chiral points to the field maximum at the center of the waveguide. The advantage of the MZI setup is its robustness against various loss mechanisms and reflection such as the insertion loss at the directional coupler and the nonunity coupling efficiency between the ridge waveguide and the PhC waveguide and between the PhC waveguide and the dipole emitter.

ACKNOWLEDGMENT

The authors thank the National Science Foundation (ECCS Grants No. 1608049 and No. 1838996) for financial support.

[1] E. Knill, R. Laflamme, and G. J. Milburn, A scheme for efficient quantum computation with linear optics, Nature (London) **409**, 46 (2001).

[2] P. Kok, W. J. Munro, K. Nemoto, T. C. Ralph, J. P. Dowling, and G. J. Milburn, Linear optical quantum computing with photonic qubits, Rev. Mod. Phys. **79**, 135 (2007).

[3] I. H. Deutsch, R. Y. Chiao, and J. C. Garrison, Diphotons in a Nonlinear Fabry-Pérot Resonator: Bound States of Interacting Photons in an Optical "Quantum Wire", Phys. Rev. Lett. **69**, 3627 (1992).

[4] Z. Cheng and G. Kurizki, Optical "Multiexcitons": Quantum Gap Solitons in Nonlinear Bragg Reflectors, Phys. Rev. Lett. **75**, 3430 (1995).

[5] P. D. Drummond and H. He, Optical mesons, Phys. Rev. A **56**, R1107 (1997).

[6] J.-T. Shen and S. Fan, Strongly Correlated Two-Photon Transport in a One-Dimensional Waveguide Coupled to a Two-Level System, Phys. Rev. Lett. **98**, 153003 (2007).

[7] J.-T. Shen and S. Fan, Strongly correlated multiparticle transport in one dimension through a quantum impurity, Phys. Rev. A **76**, 062709 (2007).

[8] Y. Shen and J.-T. Shen, Photonic-Fock-state scattering in a waveguide-QED system and their correlation functions, Phys. Rev. A **92**, 033803 (2015).

[9] O. Firstenberg, T. Peyronel, Q.-Y. Liang, A. V. Gorshkov, M. D. Lukin, and V. Vuletic, Attractive photons in a quantum nonlinear medium, Nature (London) **502**, 71 (2013).

[10] Q.-Y. Liang, A. V. Venkatramani, S. H. Cantu, T. L. Nicholson, M. J. Gullans, A. V. Gorshkov, J. D. Thompson, C. Chin,

M. D. Lukin, and V. Vuletić, Observation of three-photon bound states in a quantum nonlinear medium, Science **359**, 783 (2018).

[11] I. Söllner, S. Mahmoodian, S. L. Hansen, L. Midolo, A. Javadi, G. Kiršanskė, T. Pregnolato, H. El-Ella, E. H. Lee, J. D. Song, S. Stobbe, and P. Lodahl, Deterministic photon–emitter coupling in chiral photonic circuits, Nat. Nanotechnol. **10**, 775 (2015).

[12] R. J. Coles, D. M. Price, J. E. Dixon, B. Royall, E. Clarke, P. Kok, M. S. Skolnick, A. M. Fox, and M. N. Makhonin, Chirality of nanophotonic waveguide with embedded quantum emitter for unidirectional spin transfer, Nat. Commun. **7**, 11183 (2016).

[13] P. Lodahl, S. Mahmoodian, S. Stobbe, A. Rauschenbeutel, P. Schneeweiss, J. Volz, H. Pichler, and P. Zoller, Chiral quantum optics, Nature (London) **541**, 473 (2017).

[14] I. Friedler, D. Petrosyan, M. Fleischhauer, and G. Kurizki, Long-range interactions and entanglement of slow single-photon pulses, Phys. Rev. A **72**, 043803 (2005).

[15] J.-T. Shen and S. Fan, Coherent Single Photon Transport in a One-Dimensional Waveguide Coupled with Superconducting Quantum Bits, Phys. Rev. Lett. **95**, 213001 (2005).

[16] K. K. Y. Lee, Y. Avniel, and S. G. Johnson, Design strategies and rigorous conditions for single-polarization single-mode waveguides, Opt. Express **16**, 15170 (2008).

[17] J. T. Shen and S. Fan, Coherent photon transport from spontaneous emission in one-dimensional waveguides, Opt. Lett. **30**, 2001 (2005).

[18] Z. Wang, Y. Chong, J. D. Joannopoulos, and M. Soljacic, Observation of unidirectional backscattering-immune topological electromagnetic states, Nature (London) **461**, 772 (2009).

[19] J.-T. Shen and S. Fan, Theory of single-photon transport in a single-mode waveguide. I. Coupling to a cavity containing a two-level atom, Phys. Rev. A **79**, 023837 (2009).

[20] Z. Chen, Y. Zhou, and J.-T. Shen, Exact dissipation model for arbitrary photonic Fock state transport in waveguide QED systems, Opt. Lett. **42**, 887 (2017).

[21] Z. Chen, Y. Zhou, and J.-T. Shen, Entanglement-preserving approach for reservoir-induced photonic dissipation in waveguide QED systems, Phys. Rev. A **98**, 053830 (2018).

[22] M. Keller, B. Lange, K. Hayasaka, W. Lange, and H. Walther, Continuous generation of single photons with controlled waveform in an ion-trap cavity system, Nature (London) **431**, 1075 (2004).

[23] P. B. R. Nisbet-Jones, J. Dilley, D. Ljunggren, and A. Kuhn, Highly efficient source for indistinguishable single photons of controlled shape, New J. Phys. **13**, 103036 (2011).

[24] B. C. Pursley, S. G. Carter, M. K. Yakes, A. S. Bracker, and D. Gammon, Picosecond pulse shaping of single photons using quantum dots, Nat. Commun. **9**, 115 (2018).

[25] Y. A. Vlasov, M. O'Boyle, H. F. Hamann, and S. J. McNab, Active control of slow light on a chip with photonic crystal waveguides, Nature (London) **438**, 65 (2005).

[26] T. F. Krauss, Slow light in photonic crystal waveguides, J. Phys. D: Appl. Phys. **40**, 2666 (2007).

[27] T. Baba, Slow light in photonic crystals, Nat. Photon **2**, 465 (2008).

[28] M. Bradford and J.-T. Shen, Numerical approach to statistical properties of resonance fluorescence, Opt. Lett. **39**, 5558 (2014).

[29] Q. A. Turchette, C. J. Hood, W. Lange, H. Mabuchi, and H. J. Kimble, Measurement of Conditional Phase Shifts for Quantum Logic, Phys. Rev. Lett. **75**, 4710 (1995).

[30] J. F. Poyatos, J. I. Cirac, and P. Zoller, Complete Characterization of a Quantum Process: The Two-Bit Quantum Gate, Phys. Rev. Lett. **78**, 390 (1997).

[31] M. A. Nielsen, A simple formula for the average gate fidelity of a quantum dynamical operation, Phys. Lett. A **303**, 249 (2002).

[32] D. F. V. James, P. G. Kwiat, W. J. Munro, and A. G. White, Measurement of qubits, Phys. Rev. A **64**, 052312 (2001).

[33] K. Zyczkowski and H.-J. Sommers, Induced measures in the space of mixed quantum states, J. Phys. A: Math. Gen. **34**, 7111 (2001).

[34] D. J. Brod and J. Combes, Passive CPHASE Gate via Cross-Kerr Nonlinearities, Phys. Rev. Lett. **117**, 080502 (2016).

[35] M. Arcari, I. Söllner, A. Javadi, S. Lindskov Hansen, S. Mahmoodian, J. Liu, H. Thyrrestrup, E. H. Lee, J. D. Song, S. Stobbe, and P. Lodahl, Near-Unity Coupling Efficiency of a Quantum Emitter to a Photonic Crystal Waveguide, Phys. Rev. Lett. **113**, 093603 (2014).

[36] X. He, N. F. Hartmann, X. Ma, Y. Kim, R. Ihly, J. L. Blackburn, W. Gao, J. Kono, Y. Yomogida, A. Hirano, T. Tanaka, H. Kataura, H. Htoon, and S. K. Doorn, Tunable room-temperature single-photon emission at telecom wavelengths from sp^3 defects in carbon nanotubes, Nat. Photonics **11**, 577 (2017).